

# MODELING AND PERFORMANCE OF A SELF-EXCITED TWO-PHASE RELUCTANCE GENERATOR

E.S. Obe, I.K. Onwuka

DEPARTMENT OF ELECTRICAL ENGINEERING, UNIVERSITY OF NIGERIA, NSUKKA, NIGERIA.

## Abstract

*A self-excited two-phase reluctance generator (SETPRG) with balanced stator winding is presented. A unique balanced two-phase stator winding was designed with emphasis on obtaining a stator MMF waveform with minimum space harmonics. Then a mathematical model by which the dynamic behavior of the generator can be successfully predicted under various operating conditions is developed. The model developed accommodates balanced and unbalanced loading conditions. Self-excitation is achieved via capacitors connected across the two terminals of the stator windings. The performance of the generator under various loading conditions is studied. It is realized that the generator can simultaneously supply good voltage through its terminals, in both balanced and unbalanced load conditions within its rating. It is also observed to have a good voltage regulation. Furthermore, it was determined that the generator can accept a sudden addition of load without any transients in its output variables. However, slight transient behavior is noticed in the output variables when the generator loses load. These transients increases with increasing load power factor. The presence of these transients will not jeopardize performance as the magnitude is indeed small, nor does it pose a threat to the connected load for the same reason. The generator is also capable of re-building up its voltage after a short circuit fault is cleared.*

Keywords: ,,,,,,

## 1. Introduction

Electrical energy has become so important that any people with insufficient power available for use are classified as under-developed world. It is also a reflection of the GDP and poverty level of any particular people across the globe. Sadly, the grid power has often become inadequate, or not available in several areas, especially in remote locations. Moreover, conventional means of providing isolated power schemes is through the use of fossil fuel engines employing alternators. Not only are

these expensive and beyond the reach of the ordinary remote dwellers, it has also raised concerns on depleting fossil fuels and environmental pollution. As emphasis on non-conventional energy systems and autonomous power generation increases, a considerable interest has recently been devoted to the development of improved and appropriate generating systems. This has led to rigorous research on suitable electromechanical energy conversion devices in such power generating schemes [2-10].

The three-phase self-excited induction and reluctance machines using terminal capacitors for self excitation have received a considerable interest from researchers [2-7]. Such type of generators are attractive because of their simplicity in construction, robustness, absence of current collection brushes, low cost and near maintenance-free operation. Moreover, the three-phase induction and reluctance generators are used when high power ratings are required, whereas for small portable power sources for remote areas, single phase field-excited generators are employed. Some attention has been given to the development of self-excited single phase induction generators [8-12]. However, power supply from induction generators suffers from changes in frequency and voltage, which vary with load current. The perfection of these inherent inabilities requires additional complex schemes that would add to the cost of the machines [12]. The self-excited reluctance machine has also been researched [13-17]. However, no work has been done on the development of the two-phase reluctance generator. By two-phase, it is implied that the machine can supply single phase loads from the two stator terminals with a phase difference of 90°. Hence the present work focuses on the modeling and performance analysis of the self-excited two-phase reluctance generator, using shunt capacitors on the stator terminals for excitation. The two-phase reluctance generator studied in this work has a balanced two-phase two-pole stator winding, across which RL loads can be connected. It has unsymmetrical rotor (that is, saliency in the rotor), and uniform poles. The rotor is equipped with only short-circuited windings called damper windings. In this work, computer simulation of the developed model of the generator is done in the MATLAB/SIMULINK environment [18] and closely studied for different loading conditions. The results of these simulations are then analyzed.

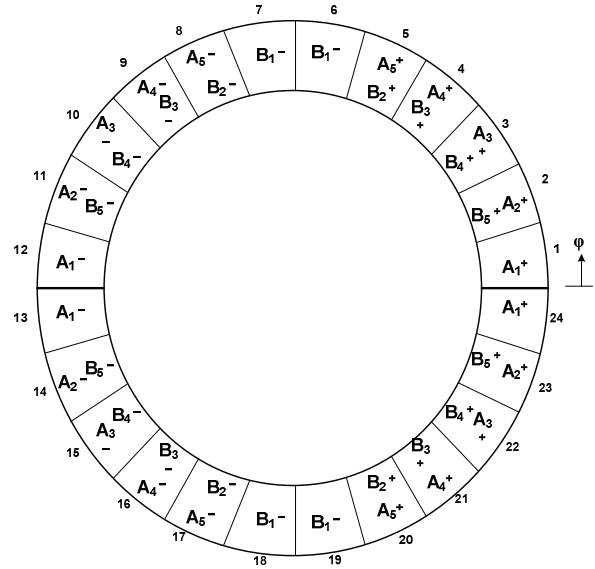


Figure 1: Machine stator winding clock diagram.

## 2. Stator Winding and Inductances

### 2.1. Winding design

Of the several types of stator windings in use, the integral-slot, chorded, double layer winding is developed for this work. The clock diagram is presented in Figure 1. The following properties will be observed: Number of slots = 24; Phase spread = 150°; Pole-pitch = 12 slots per pole; Coil pitch = 7 slots average; Slot angular pitch = 15°; Phase shift = 90°; Phase belt = 10 slot pitch pitches. The number of conductors per slot is 18, and the slots carry equal number of conductors.

### 2.2. Winding function

Owing to the sinusoidal nature of the windings obtained in Figure 1, the winding function (WF) methodology developed in [21] is adopted for inductance calculation. The fundamental components of the winding functions for the two stator windings are:

$$\begin{aligned} N_{as} &= N_p \cos(\phi_s) \\ N_{bs} &= N_p \sin(\phi_s) \end{aligned} \quad (1)$$

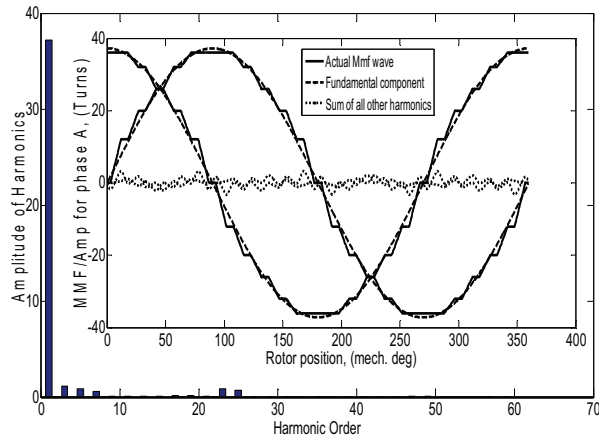


Figure 2: Plot of the winding function, its fundamental component and harmonic spectrum.

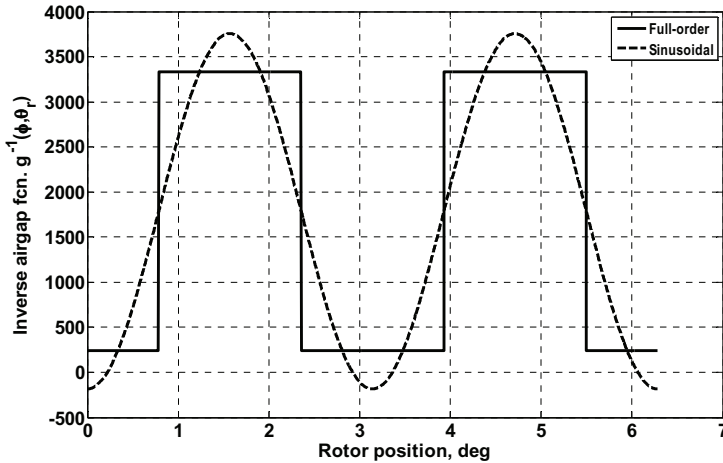


Figure 3: The inverse airgap functions.

### 2.3. Air gap function

The saliency of the rotor is considered in determining the air gap function. This is given as:

$$g^{-1}(\phi_s, \theta_r) = \alpha_1 + \alpha_2 \cos 2(\phi_s, \theta_r) \quad (2)$$

where:

$$(3)$$

$$(4)$$

and  $g_1$  is the minimum air gap length,  $g_2$  is maximum air gap length and  $\beta$  is the pole arc/pole pitch ratio.

Substituting the parameters values of the Appendix into (2), the inverse air gap function will be obtained as:

$$g^{-1}(\phi_s) = 1373.3 + 1977.8 \cos 2(\phi_s - \theta_r) \quad (5)$$

### 2.4. The magnetizing inductance (without saturation effect)

The WF formula for calculating inductance  $L_{xy}$  between two windings  $x$  and  $y$  is:

$$L_{xy} = \mu_o r l \int_0^{2\pi} N_x(\phi_s) N_y(\phi_s) g^{-1}(\phi_s, \theta_r) d\phi_s \quad (6)$$

Noting that the air gap length is now a function of  $(\phi_s, \theta_r)$ , and substituting (1) and (2) into (6) we obtain the magnetizing inductances on the  $a$ - and  $b$ - phases as:

$$L_{asas} = \mu_o r l \pi C_1^2 \left( \alpha_1 - \frac{\alpha_2}{2} \cos 2\theta_r \right) \quad (7)$$

$$L_{bsbs} = \mu_o r l \pi C_1^2 \left( \alpha_1 - \frac{\alpha_2}{2} \cos 2\theta_r \right) \quad (8)$$

$$L_{asbs} = \mu_o r l \pi C_1 C_2 \frac{\alpha_2}{2} \sin 2\theta_r \quad (9)$$

It is clear that reciprocity holds since the order of the two winding functions can be interchanged. Hence,  $L_{asbs} = L_{bsas}$  Using the parameter values of the Appendix the inductance values were computed for the fundamental value of the winding function and shown in Figure 4. If the leakage inductances are included in the phases, the self inductances become:

$$L_{as} = L_{ls} + L_{asas} \quad (10)$$

and

$$L_{bs} = L_{ls} + L_{bsbs} \quad (11)$$

## 3. Machine Model

Figure 5 shows the schematic connection diagram for the system under study. A more detailed analysis is presented in [1]. The following assumptions are made in the model development:

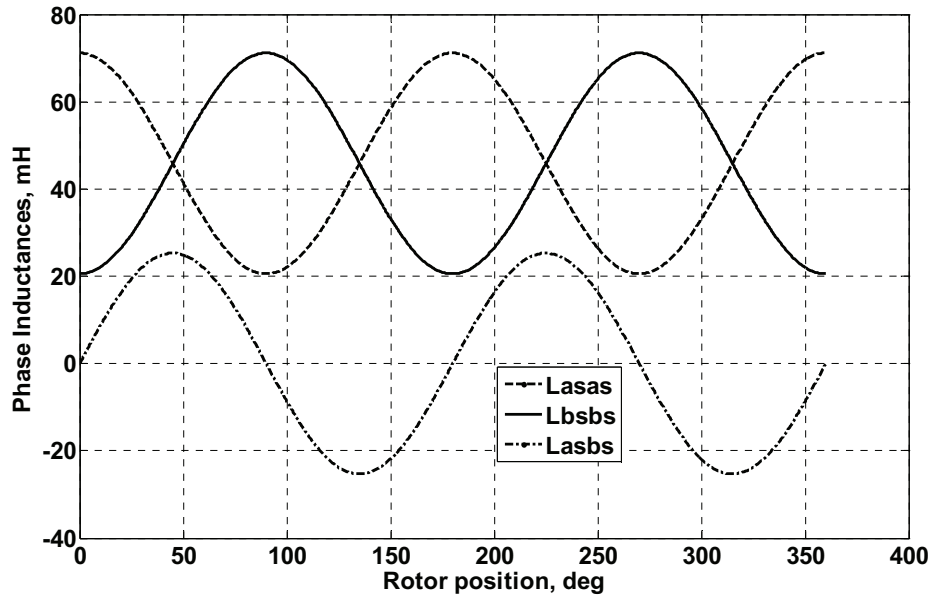


Figure 4: The variation of stator inductances with  $\theta_r$ .

- All the machine parameters, except the  $d$ -axis magnetizing inductance are assumed to be constant. Only the  $d$ -axis magnetizing inductance is assumed to be affected by saturation.
- A residual magnetism of 0.005 Teslas exists on the rotor  $d$ -axis.
- The core loss in the machine is ignored.
- The MMF space harmonics and the time harmonics in the induced voltage and current waveforms are ignored.
- The  $d - q$  axis reference frame is fixed in the rotor, which rotates at a constant speed of  $\omega_r$ .
- The generator is driven by a constant speed motor at 3000rpm.

With the rotor variables referred to the stator, the voltage equations become:

$$\begin{aligned}
 V_{as} &= -r_s i_{as} + p\lambda_{as} \\
 V_{bs} &= -r_s i_{bs} + p\lambda_{bs} \\
 \dot{V}_{kd} &= -\dot{r}_{kd} i_{kd} + p\dot{\lambda}_{kd} \\
 \dot{V}_{kq} &= -\dot{r}_{kq} i_{kq} + p\dot{\lambda}_{kq}
 \end{aligned} \tag{12}$$

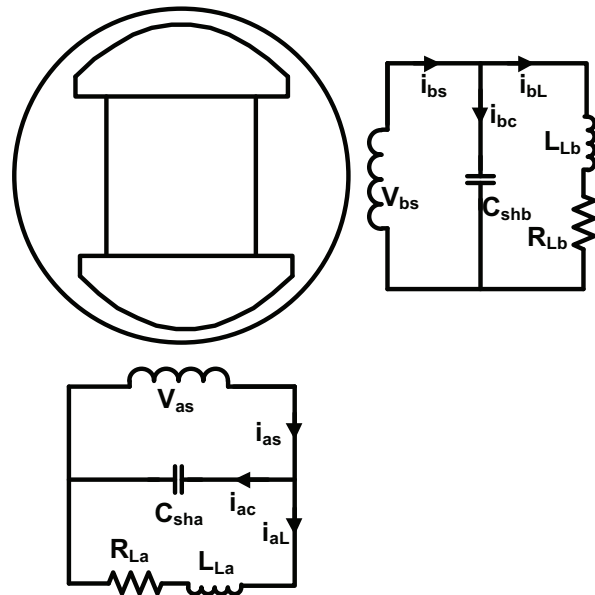


Figure 5: The general schematic diagram of the SETPRG. The damper windings were excluded in this diagram for simplicity.

The negative sign of the stator currents indicates that they flow out of the stator terminals. The flux linkages are described by the following equations:

$$\begin{bmatrix} \lambda_{abs} \\ \dot{\lambda}_{kdkq} \end{bmatrix} = \begin{bmatrix} L_s & \dot{L}_{sr} \\ (\dot{L}_{sr})^T & \dot{L}_{kdkq} \end{bmatrix} \begin{bmatrix} -i_{abs} \\ \dot{i}_{kdkq} \end{bmatrix} \quad (13)$$

where

$$\begin{aligned} L_s &= \begin{bmatrix} L_{asas} & L_{asbs} \\ L_{asbs} & L_{bsbs} \end{bmatrix} \\ L_{sr} &= \begin{bmatrix} L_{askd} & L_{askq} \\ L_{bskd} & L_{bskq} \end{bmatrix} \\ L_{kdkq} &= \begin{bmatrix} L_{kd} & 0 \\ 0 & L_{kq} \end{bmatrix} \end{aligned} \quad (14)$$

$$\begin{aligned} L_{kd} &= L_{lkd} + L_{md} \\ L_{kq} &= L_{lkq} + L_{mq} \end{aligned} \quad (15)$$

$$\begin{aligned} [\lambda_{abs}] &= \begin{bmatrix} \lambda_{as} \\ \lambda_{bs} \end{bmatrix}, \\ [\dot{\lambda}_{kdkq}] &= \begin{bmatrix} \dot{\lambda}_{kd} \\ \dot{\lambda}_{kq} \end{bmatrix}, \\ [i_{abs}] &= \begin{bmatrix} i_{as} \\ i_{bs} \end{bmatrix}, \\ [\dot{i}_{kdkq}] &= \begin{bmatrix} \dot{i}_{kd} \\ \dot{i}_{kq} \end{bmatrix} \end{aligned} \quad (16)$$

The *a*- and *b*- phase stator currents are given by:

$$\begin{aligned} i_{as} &= i_{la} + pQ_a \\ i_{bs} &= i_{lb} + pQ_b \end{aligned} \quad (17)$$

where *Q*<sub>a</sub> and *Q*<sub>b</sub> are the charges on the capacitors on the *a*- and *b*-phases, given by:

$$\begin{bmatrix} Q_a \\ Q_b \end{bmatrix} = \begin{bmatrix} C_{sha} & 0 \\ 0 & C_{shb} \end{bmatrix} \begin{bmatrix} V_{as} \\ V_{bs} \end{bmatrix} \quad (18)$$

*C*<sub>sha</sub> and *C*<sub>shb</sub> are the capacitances of the shunt capacitors used in *a*- and *b*-phases respectively. To simplify the analysis process, the time varying inductances associated with

(7) - (12) are eliminated via a change of variables, in this case, from the stationary two-phase machine variables to the *d* - *q* variables of a reference frame fixed in the rotor.

The rotor of a salient-pole synchronous machine is magnetically unsymmetrical. The rotor variables are displaced from each other by an angle of 90°, along the *d*- and *q*-axes. Hence a change of variables for the rotor variables will offer no advantage. However, it will be very beneficial for the stator variables [20]. The transformation is defined by:

$$\begin{bmatrix} F_d \\ F_q \end{bmatrix} = K_{2s} \begin{bmatrix} F_{as} \\ F_{bs} \end{bmatrix} \quad (19)$$

where *F* represents any variable such as voltage, current, flux linkages, or electric charge. The *d* - *q*, rather than the usual *d* - *q* transformation matrix is used. Along with its inverse (*k*<sub>2s</sub>)<sup>-1</sup> it is given by:

$$\begin{aligned} K_{2s} &= \begin{bmatrix} \sin \theta_r & -\cos \theta_r \\ \cos \theta_r & \sin \theta_r \end{bmatrix} \text{ and} \\ (K_{2s})^{-1} &= \begin{bmatrix} \sin \theta_r & \cos \theta_r \\ -\cos \theta_r & \sin \theta_r \end{bmatrix} \end{aligned} \quad (20)$$

Also,

$$F_{dq} = \begin{bmatrix} F_d \\ F_q \end{bmatrix} \quad (21)$$

Applying (20) to the stator equation in (12), the voltage equations become:

$$\begin{aligned} V_{ds} &= -r_s i_{ds} - \omega_r \lambda_{qs} + p \lambda_{ds} \\ V_{qs} &= -r_s i_{qs} - \omega_r \lambda_{ds} + p \lambda_{qs} \end{aligned} \quad (22)$$

$$\begin{aligned} \dot{V}_{kd} &= \dot{r}_{dk} \dot{i}_k + p \dot{\lambda}_{kd} \\ \dot{V}_{kq} &= \dot{r}_{kq} \dot{i}_{kq} + p \dot{\lambda}_{kq} \end{aligned} \quad (23)$$

Note that that the rotor voltages are not affected.

Also, the transformed flux linkages are obtained as:

$$\begin{bmatrix} \lambda_{ds} \\ \lambda_{qs} \\ \dot{\lambda}_{kd} \\ \dot{\lambda}_{kq} \end{bmatrix} = \begin{bmatrix} L_{ls} + L_{md} & 0 & L_{md} & 0 \\ 0 & L_{ls} + L_{md} & 0 & L_{md} \\ L_{md} & 0 & L_{lkd} + L_{md} & 0 \\ 0 & L_{mq} & 0 & L_{lkq} + L_{mq} \end{bmatrix} \quad (24)$$

The  $d$ - and  $q$ -axes currents can be obtained by a simultaneous solution of (24). The transformed currents and charges of (18) become:

$$pQ_{ds} = \omega_r Q_{qs} - i_{dl} + i_{ds} \quad (25)$$

$$pQ_{qs} = \omega_r Q_{ds} - i_{ql} + i_{qs} \quad (26)$$

If  $S_a$  and  $S_b$  are defined by:

$$\begin{bmatrix} S_a \\ S_b \end{bmatrix} = \begin{bmatrix} \frac{L_{al}}{R_{al}} & 0 \\ 0 & \frac{L_{bl}}{R_{bl}} \end{bmatrix} \begin{bmatrix} i_{al} \\ i_{bl} \end{bmatrix} \quad (27)$$

The load currents will be given by:

$$\begin{bmatrix} i_{al} \\ i_{bl} \end{bmatrix} = \begin{bmatrix} \frac{1}{R_{al}} & 0 \\ 0 & \frac{1}{R_{bl}} \end{bmatrix} \begin{bmatrix} V_{as} \\ V_{bs} \end{bmatrix} - p \begin{bmatrix} S_a \\ S_b \end{bmatrix} \quad (28)$$

Applying (20) to (28) will give a resultant equation of:

$$\begin{aligned} pS_{ds} &= \omega_r S_{qs} + i_{dd} - i_{ld} \\ pS_{qs} &= \omega_r S_{ds} + i_{qq} - i_{lq} \end{aligned} \quad (29)$$

where,

$$\begin{aligned} i_{qq} &= (t_1 - t_2 \cos 2\theta_r) V_{ds} - (t_2 \sin 2\theta_r) V_{qs} \\ i_{dd} &= (t_2 \sin 2\theta_r) V_{ds} - (t_1 - t_2 \cos 2\theta_r) V_{qs} \end{aligned} \quad (30)$$

$$\begin{bmatrix} S_{ds} \\ S_{qs} \end{bmatrix} = \begin{bmatrix} L_1 - L_2 \cos 2\theta_r & L_2 \sin 2\theta_r \\ L_2 \sin 2\theta_r & L_1 + L_2 \cos 2\theta_r \end{bmatrix} \begin{bmatrix} i_{dl} \\ i_{ql} \end{bmatrix} \quad (31)$$

where,

$$\begin{aligned} t_1 &= \frac{1}{2} \left( \frac{1}{R_{al}} + \frac{1}{R_{bl}} \right) \\ t_2 &= \frac{1}{2} \left( \frac{1}{R_{al}} - \frac{1}{R_{bl}} \right) \end{aligned} \quad (32)$$

$$\begin{aligned} L_1 &= \frac{1}{2} \left( \frac{L_{al}}{R_{al}} + \frac{L_{bl}}{R_{bl}} \right) \\ L_2 &= \frac{1}{2} \left( \frac{L_{al}}{R_{al}} - \frac{L_{bl}}{R_{bl}} \right) \end{aligned} \quad (33)$$

The dependence of (30) and (31) on  $\theta_r$  is to allow for the assessment of unbalanced loading effects. It is easy to see that if  $R_{al} = R_{bl}$  then  $t_1 = L_2$  and hence the dependence on  $\theta_r$  will vanish.

The complex power developed is given by:

$$S = (V_{ds} + jV_{qs})(i_{ds} - ji_{qs}) \quad (34)$$

Hence, the performance of the machine for different loading conditions can be analyzed.

## 4. Results and discussion

The machine was simulated on the MATLAB/SIMULINK environment. Self-excitation was achieved using excitation capacitance of  $117.1\mu\text{F}$  on both stator windings. The principle underlying the self-excitation of the machine is a well known phenomenon, dependent on the existence of remnant flux and magnetic saturation similar to that of the induction generators. The frequency,  $f$ , of the generated voltage is determined by:

$$f = \frac{N_r P}{120} \quad (35)$$

where,  $N_r$  and  $P$  are the rotor speed and number of poles respectively. This frequency is determined to be 50Hz, and was found to correspond with that of the generated voltage.

### 4.1. Build-up characteristics

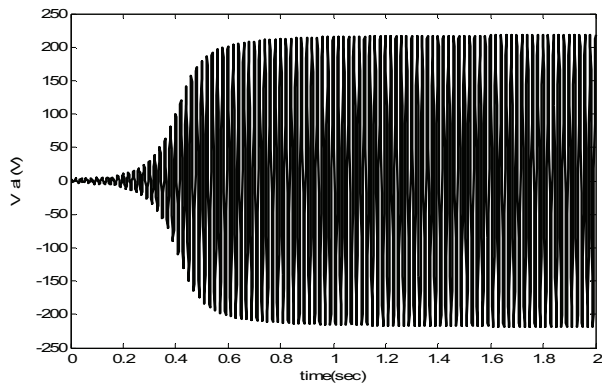
The build-up characteristics of the machine at no-load is shown in Figure 6. It is observed that the terminal voltage is 218.5V at a frequency of 50Hz. Also, the no-load current is almost zero, as all of the stator current passes through the excitation capacitors at no-load.

### 4.2. Load characteristics

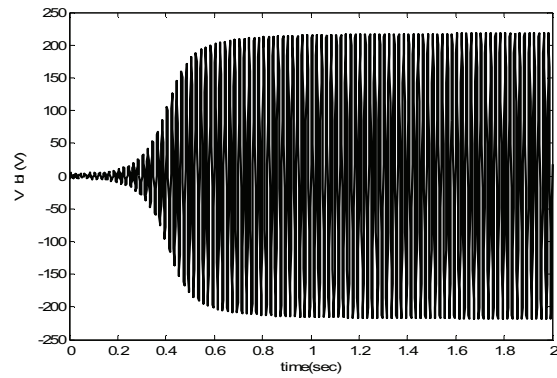
The load characteristics here is deduced by loading the generator gradually from no-load to full load until it reaches pull-out. For a particular fixed power factor loading, only the value of the load resistance is adjusted, and the corresponding load inductance needed for that particular load power factor are calculated according to the equation:

$$L_l = \frac{R_l}{\omega_l} \sqrt{\left( \left( \frac{1}{\cos \theta} \right)^2 - 1 \right)} \quad (36)$$

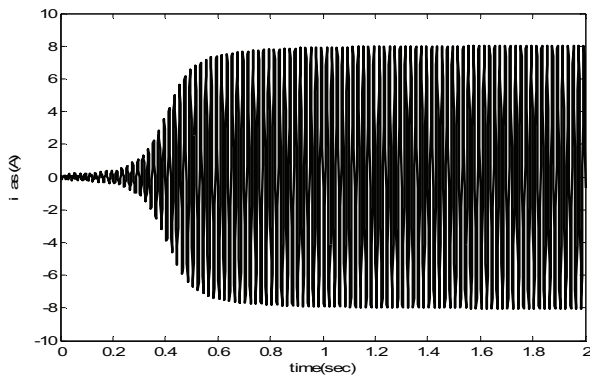
The results obtained are shown in Figure 7 where it is observed that the higher the power factor, the more power the generator is able to



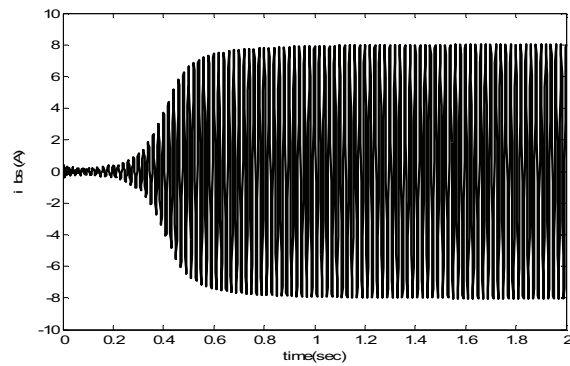
(a) No-load a-phase voltage



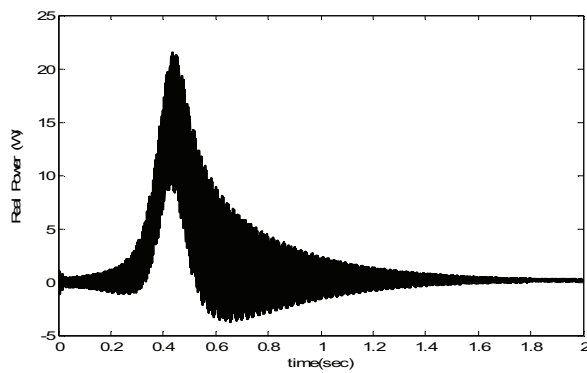
(b) No-load b-phase voltage



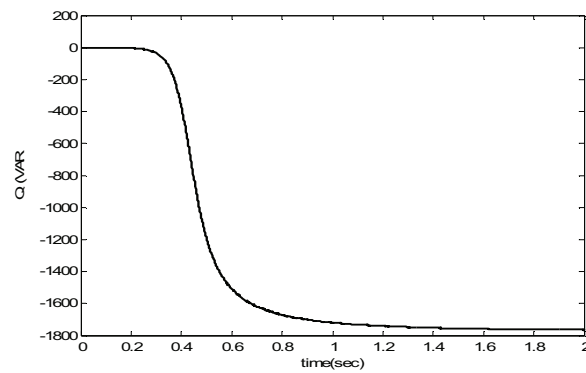
(c) No-load stator a-phase current



(d) No-load stator b-phase current

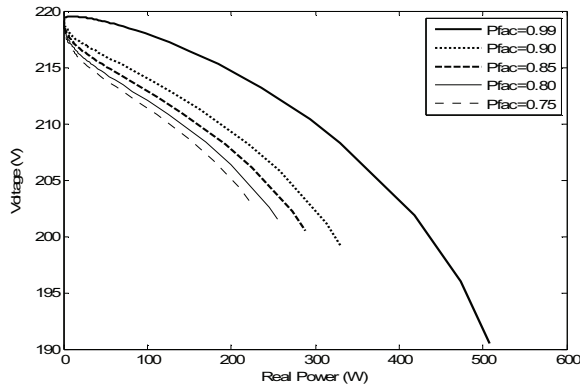


(e) No-load real power

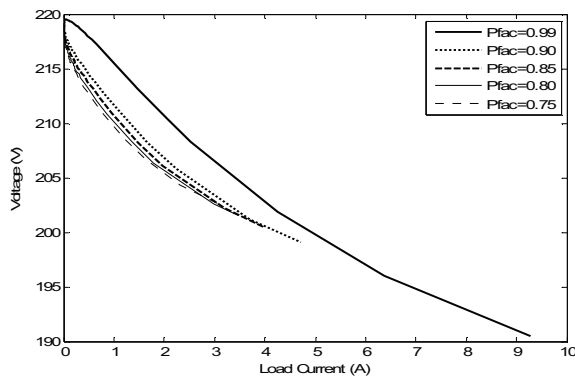


(f) No-load reactive power

Figure 6: Build-up characteristics of the SETPRG under no-load.



(a) Load voltage vs real power



(b) Load voltage vs load current

Figure 7: Load characteristics of the SETPRG

deliver at a particular voltage. Generally, for a given voltage, the load current is more with increasing load power factor. This can provide information for loading the generator.

### 4.3. Transient loading and loss of load performance

To determine the transient loading and loss of load behavior of the generator at different power factor conditions, the object of observation is the envelope of the terminal wave form. First the generator builds up a voltage at no-load at its terminals when suddenly a load is added at a time  $t = 5.0$  sec for 2 seconds. The responses are shown in Figure 8.

Transients are observed at the load voltages only at the loss of load, which increases with increasing load power factor. The absence of

transients in the load currents, both at the addition and removal of load is equally observed.

### 4.4. Short-circuit at terminals of stator winding

The generator terminals were suddenly shorted from an open circuit condition, for a period of 0.1 seconds, and then the short circuit condition was cleared. The short-circuit was performed with a load resistance of  $70\Omega$  at a power factor of 0.99 lagging. This characteristic is represented in Figure 9. It is observed that the machine is able to build up voltage again after a complete voltage collapse. The terminal voltages are represented by both their sinusoidal forms and their upper envelopes, for clarity.

#### 4.4.1. Unbalanced loading of the terminals

This was considered for different power factor conditions, at a constant load resistance of  $70\Omega$ . First, the load is suddenly applied on the a-phase at time  $t = 5$ s for 2 seconds, keeping the b-phase open all the while. Afterwards, the condition was reversed for the two windings. The load voltage and current response to these conditions is represented in Figure 10, considering again, the upper envelopes. It is observed that the presence of transients only occur at the loss of load, with degrees increasing with the power factor value. The load current of the phase with more load rises to a significant value, while the other phase load current is less than 2mA, approximately zero. The transient observed in the load current of the unloaded phase is only for the 0.99 power factor, the rest has no transients. These are shown in Figure 11.

## 5. Conclusion

Energy transferred across the air gap of a magnetically coupled electromagnetic system is given by:

$$W_f = \int \sum_{j=1}^n i_j d\lambda_j \quad (37)$$

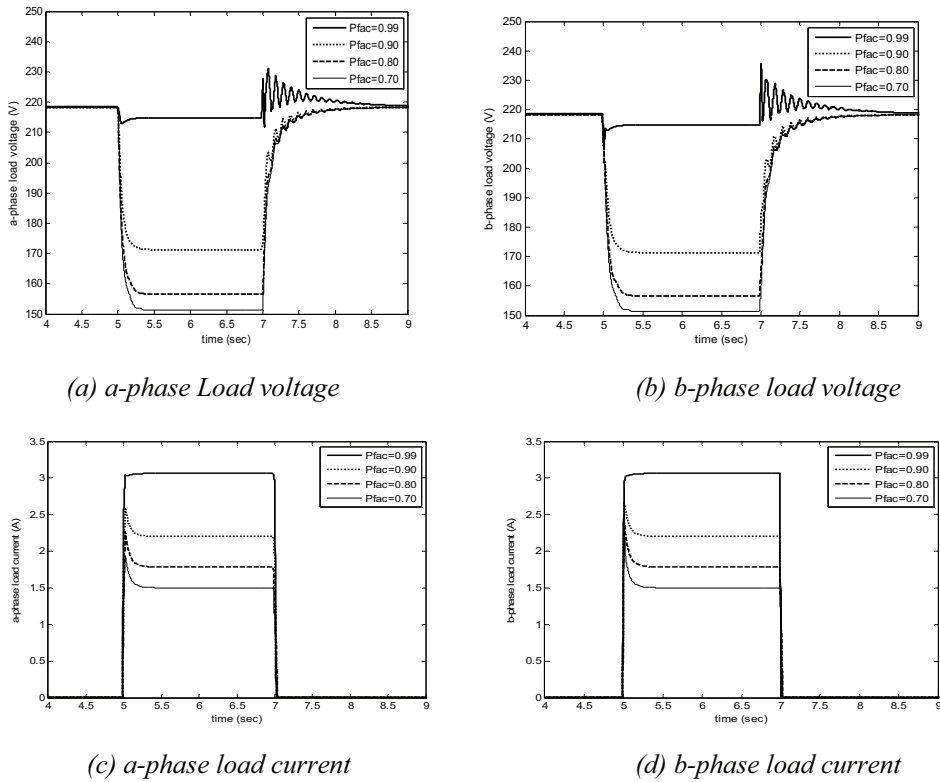


Figure 8: Sudden addition and loss of load of the SETPRG; (a) and (b) are the upper envelopes of the *a*- and *b*-phase load voltages, (c) and (d) upper envelopes of the *a*- and *b*-phase load currents, respectively.

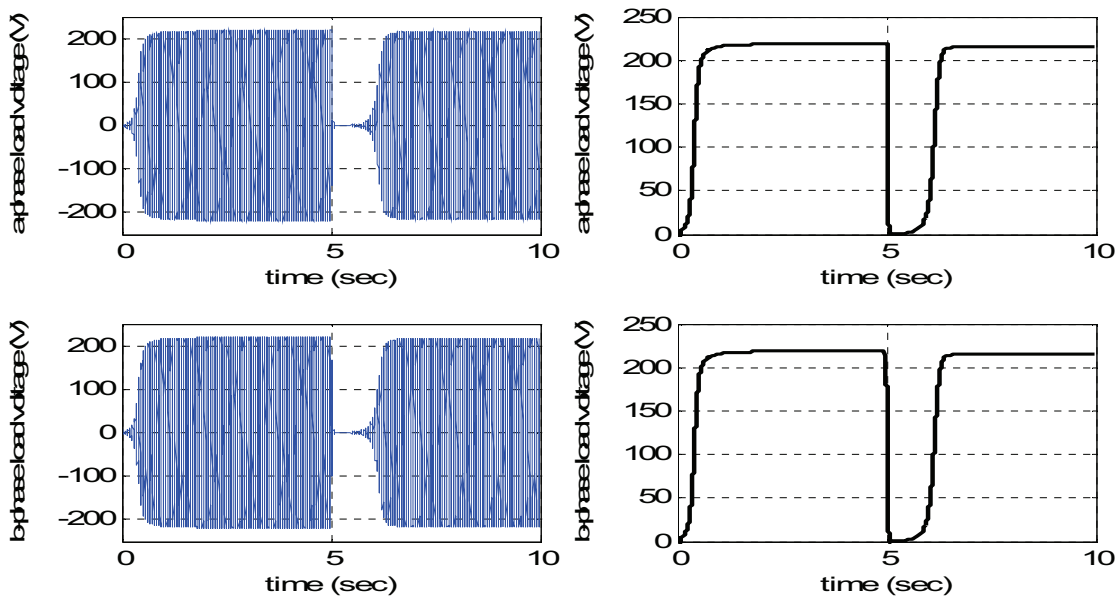


Figure 9: Re-building up process after removing a short circuit fault: (a) *a*-phase Load voltage (sinusoidal), (b) *a*-phase Load voltage (upper envelope), (c) *b*-phase Load voltage (sinusoidal), (d) *b*-phase Load voltage (upper envelope).

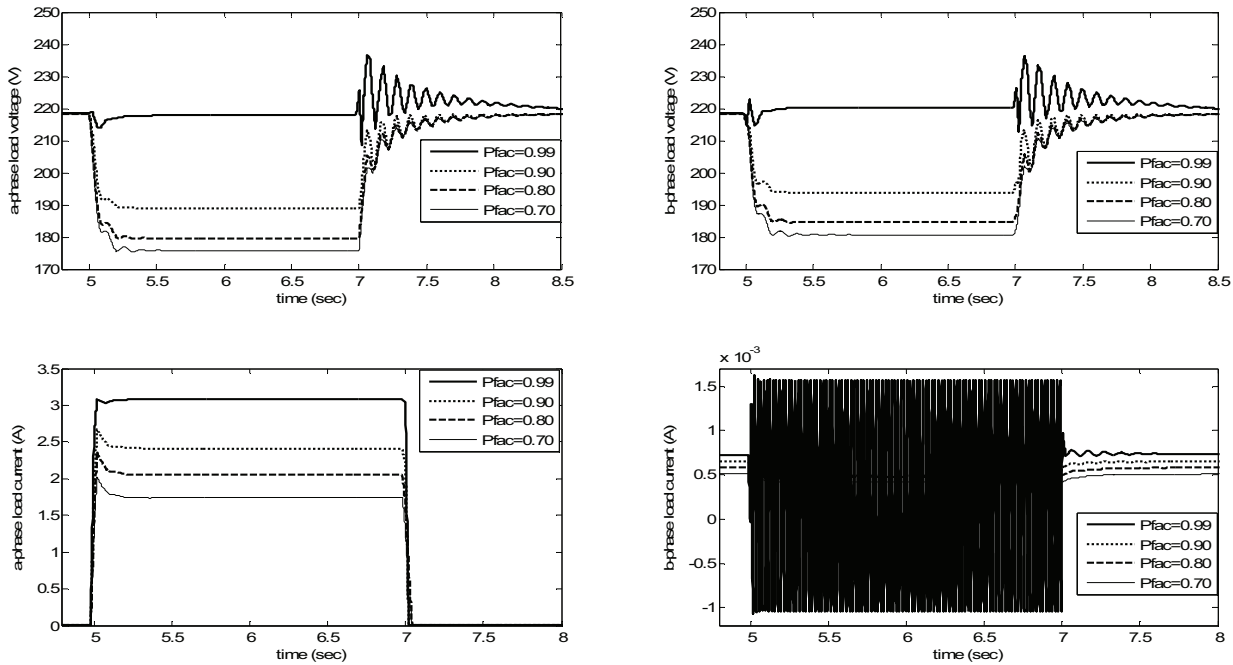


Figure 10: Unbalanced loading effects (a) *a*-phase load voltage, (b) *b*-phase load voltage, (c) *a*-phase load current, (d) *b*-phase load current.

This shows a dependence on the flux linkage  $\lambda$  [21], which in turn depends on the winding function. Winding function depends on the turns function (which represents the number of turns of a particular winding). A balanced stator winding is involved in the SET-PRG discussed in this work. Unlike the unbalanced system used by all single phase systems, it is seen that this presents a better utilization of the stator core and slots. Balanced stator windings will take more copper than unbalanced stator windings, which will interact with the magnetic flux in the air gap to transfer more power across it. Finally the Self-Excited Two-Phase Reluctance Generator when fully developed could be preferred to the Self-Excited Single-Phase Reluctance Generator of the same size for higher power capability, loss of load behavior, and robustness.

## References

1. Onwuka, I. K. *Modeling and performance of a self-excited two-phase reluctance generator*, M. Eng Thesis, Dept of Electrical Engineering, University of Nigeria, Nsukka.
2. A. K. Tandon, S. S. Murthy, and G. J. Berg. Steady-state analysis of capacitor self-excited induction generators, *IEEE Transactions on Power Apparatus and Systems*, vol. PAS-103, no. 3, pp. 612-618, March 1984.
3. N. H. Malik, and A. A. Mazi. Capacitance requirements for isolated self-excited induction generators, *IEEE Transactions on Energy Conversion*, vol.2, no. 1, pp. 62-69, March 1987.
4. C. Grantham, D. Sutanto, and B. Mismail. Steady-state and transient analysis of self-excited induction generators, *IEE Proceedings*, vol. 136, pt. B, no. 2, pp. 61-68, March 1989.

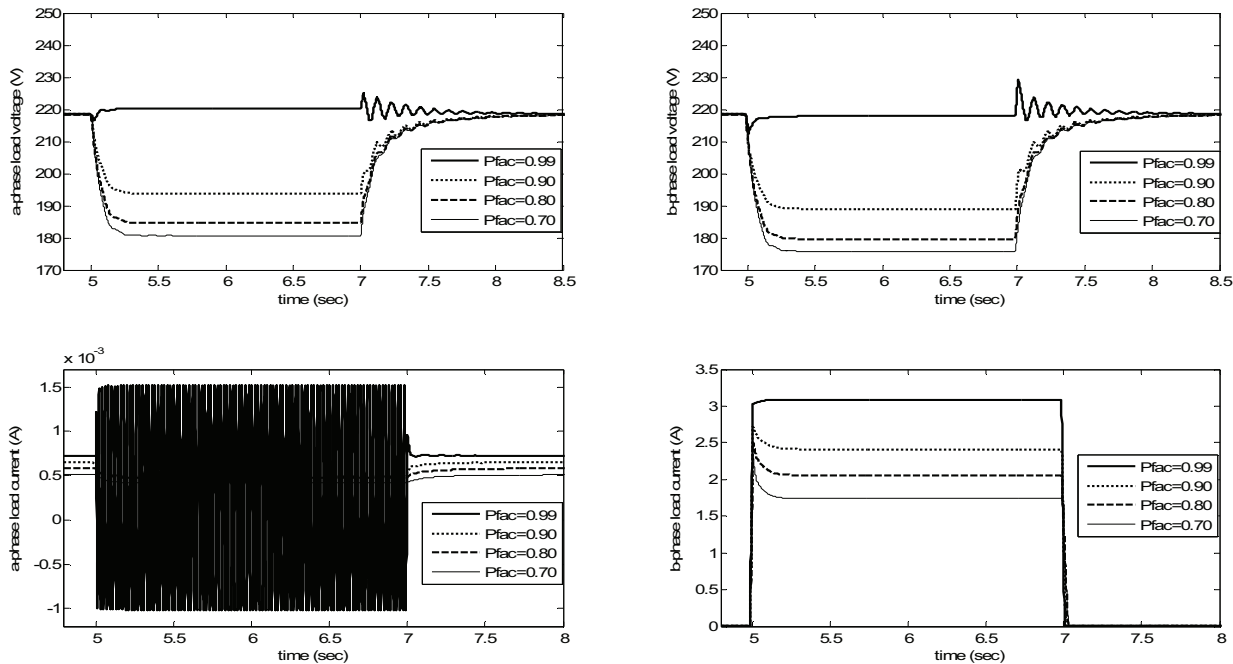


Figure 11: Terminal voltage and current response to unbalanced terminal loading (a)  $a$ -phase load voltage, (b)  $b$ -phase load voltage, (c)  $a$ -phase load current, (d)  $b$ -phase load current.

5. T. F. Chan. Steady-state analysis of a three-phase self-excited reluctance generators, *IEEE Transactions on Energy Conversion*, vol. 7, no. 1, pp. 223-230, March 1992.
6. Y. H. A. Rahim, A. L. Mohamadien, and A.S. Al Kalaf. Comparison between the Steady State performance of the self-excited reluctance and induction generators, *IEEE Transactions on Energy Conversion*, vol. 5, no. 3, pp 519-525, Sept 1990.
7. A. M. Osheiba and M. A. Rahman. Performance analysis of self-excited induction and reluctance generators, *Electric Machines Power System*, vol. 19, no. 4, pp477-499, 1991.
8. O. Ojo and I. Bhat. An analysis of single-phase self-excited induction generators: Model development and steady state calculations, *IEEE Trans. on Energy Conversion*, vol. 10, no. 2, pp. 254-260, June 1995.
9. O. Ojo. The transient and qualitative performance of a self-excited single-phase induction generator, *IEEE Trans. on Energy Conversion*, vol. 10, no. 3, pp. 493-501, September 1995.
10. O. Ojo. Performance of a self-excited single-phase induction generators with shunt, short-shunt and long-shunt excitation connections, *IEEE Transaction on Energy Conversion*, vol. 11, no. 3, pp. 477-482, September 1996.
11. Bhim Singh, L. B. Shilpakar, S. S. Murthy, and A. K.Tiwari. Improved steady state and transient performance with optimum excitation of single-phase self-excited induction generator, *Electric Machines and Power Systems*, 28:591-604, 2000.
12. Obasohan I. Omozusi. *Dynamics and control of a battery inverter single-phase induction generator system*. M.Sc thesis presented to the Faculty of Graduate School

- Tennessee Technological University, Dec 1998.
13. J. W. Finch and P. J. Lawrenson. Synchronous performance of single-phase reluctance motors, *Proc. Inst. Electrical Engineering*, vol.125, no. 12, pp. 1350-1356, December 1978.
  14. J. W. Finch and P. J. Lawrenson. Asynchronous performance of single-phase reluctance motors, *Proc. Inst. Electrical Engineering*, vol.126, no. 12, pp. 549-562, December 1979.
  15. J. Chen and P. Famouri. Single-phase self-excited reluctance generator, part I: Steady-state analysis, *Electr. Power Component Systems*, vol. 31, pp. 129-147, 2003.
  16. S. M. Allam, M. A. El-Khazendar, and A. M. Osheiba. Dynamic analysis of a self-excited single-phase reluctance generator, *Electric Power Components and Systems*, 34:725-738, 2006.
  17. S. M. Allam, M. A. El-Khazendar, and A. M. Osheiba. Steady-state analysis of a self-excited single-phase reluctance generator, *IEEE Transactions on Energy Conversion*, vol. 22, no. 3, Sept 2007.
  18. MATLAB. *Mathworks 2007*: Natic, Pennsylvania, USA.
  19. Erwin Kreyszig. *Advanced Engineering Mathematics*, John Wiley and Sons, Inc, New York, 1979.
  20. Paul C. Krause, Oleg Wasynczuk, Scott D. Sudhoff. *Analysis of Electric Machinery*, IEEE Press, New York, 1995.
  21. Obe, E. S. Nnadi, D. B and Eke, J. Inductances and Airgap Flux density of a Synchronous Reluctance Machine using the Actual Machine Geometry, *NSE Technical Trans.* Vol. 44. No. 4, pp.49-63, 2009.

axial length of the air gap,  $l = 0.06m$ .

#### 2. Machine Parameters.

$r_s = 1.50$ ;  $r_{kd} = 2.25$ ;  $r_{kq} = 2.30$ ;  $L_{mq} = 0.0213$ ;  
 Unsaturated value of  $L_{md} = 0.1309$ ;  
 $L_{ls} = 0.0099$ ;  $L_{ld} = 0.0010$ ;  $L_{lkq} = 0.0010$ ;  
 $C_{sha} = C_{shb} = 117.1\mu F$ ;  $\omega_r = 314.1593\text{rad/sec}$ .

## Appendix

#### 1. Stator Parameters.

$g_1 = 0.0003$ ;  $g_2 = 50 * g_1$ ;  $\alpha = 0.6$ ;  $\theta = 410 - 7$ ;  
 mean radius of the air gap,  $r = 0.075m$ ;